Journal of Power Sources 206 (2012) 421–428

Contents lists available at SciVerse ScienceDirect

Journal of Power Sources

journal homepage: www.elsevier.com/locate/jpowsour

Analysis of pressure variations in a low-pressure nickel–hydrogen battery. Part 2: Cells with metal hydride storage

B.K. Purushothaman*, J.S. Wainright

Department of Chemical Engineering, Case Western Reserve University, 10900 Euclid Avenue, Cleveland, OH 44106, USA

ARTICLE INFO

Article history:
Received 16 January 2012
Received in revised form 27 January 2012
Accepted 27 January 2012
Available online 7 February 2012

Keywords:
Nickel hydrogen battery
State of charge
Fuel gauging
Metal hydride
Pressure analysis

ABSTRACT

A sub-atmospheric pressure nickel hydrogen ($Ni–H_2$) battery with metal hydride for hydrogen storage is developed for implantable neuroprosthetic devices. Pressure variations during charge and discharge of the cell are analyzed at different states of charge and are found to follow the desorption curve of the pressure composition isotherm (PCI) of the metal hydride. The measured pressure agreed well with the calculated theoretical pressure based on the PCI and is used to predict the state of charge of the battery. Hydrogen equilibration with the metal hydride during charge/discharge cycling is fast when the pressure is in the range from 8 to 13 psia and slower in the range from 6 to 8 psia. The time constant for the slower hydrogen equilibration, 1.37 h, is similar to the time constant for oxygen recombination and therefore pressure changes due to different mechanisms are difficult to estimate. The self-discharge rate of the cell with metal hydride is two times lower in comparison to the cell with gaseous hydrogen storage alone and is a result of the lower pressure in the cell when the metal hydride is used.

1. Introduction

In the 2nd part of this paper the performance of the nickel–hydrogen cell using a metal hydride for hydrogen storage will be discussed. Metal hydride technology was developed in the 1970s for hydrogen storage applications. Subsequently metal hydrides gained particular interest owing to their potential application as a negative electrode to replace cadmium in nickel–cadmium batteries [1–13]. Metal hydrides are intermetallic compounds generally consisting of one strong hydride forming element (A) and one weak hydride forming element (B). Commonly used hydrogen storage alloys are typically either (1) a wide set of alloys composed of rare earth elements with nickel (AB_5 type systems) or (2) alloys of zirconium, vanadium, magnesium and/or titanium with nickel (A_2B, AB or AB_2 type systems). Various hydrogen storage alloy systems used as metal hydride negative electrodes are reviewed by Kleperis et al. [12] and Feng et al. [13].

The performance of the metal hydride electrodes is measured in terms of their capacity, cycle life and power density. These capabilities are determined by the kinetics of the processes occurring at the electrode/electrolyte interface and the rate of hydrogen diffusion in the bulk of the alloy. For good cycle life, the metal hydride electrodes should exhibit good oxidation resistance in alkaline electrolyte and when exposed to oxygen gas. The chemical elements of the metal hydride in highly concentrated alkaline electrolyte often react to form oxides (e.g., lanthanum oxide [13–16], magnesium oxide [17,18]) and fail to store hydrogen reversibly. In some aluminum containing metal hydride systems, aluminum can dissolve [19] and migrate to the positive electrode. In our low pressure $Ni–H_2$ battery, the metal hydride functions as hydrogen storage material alone and is not an electrode as in a NiMH battery. A platinum catalyzed, gas-fed electrode serves as the negative electrode in the cell. The metal hydride is physically and electrically separated from both electrodes and the electrolyte in the $Ni–H_2$ cell. This should significantly reduce the oxidation and enhance the cycle life of the metal hydride. The metal hydride used in our $Ni–H_2$ cell is $LaAl_{0.3}Ni_{4.7}$ surface modified by Pd and was developed at CWRU [20–22]. Addition of palladium to the metal hydride minimizes the formation of $Mg(OH)_2$ and $La(OH)_2$ [18] and the dissolution of aluminum which should further enhance the life of the metal hydride.

The other factor that increases the corrosion of the metal hydrides is commonly referred as particle pulverization or decrepitation (breaking of particles) [13,19,23]. Metal hydrides have a high storage capacity and the large molar volume of hydrogen in the hydride phase induces large volume changes upon cycling. As a result the particles pulverize rapidly, breaking into smaller particles. This results in increased particle to particle contact resistance and increased polarization resistance when used as the negative electrode in a conventional NiMH battery [24]. The increase in the polarization resistance is due to the decrease in the

* Corresponding author at: Medtronic, Mounds View North Facility, 8200 Coral Sea Street NE, MVN51, Mounds View, MN 55112, USA. Tel.: +1 763 526 0193; fax: +1 763 526 5737.
E-mail addresses: bushan.k.purushothaman@medtronic.com, bushan@gmail.com (B.K. Purushothaman).

0378-7753/$ – see front matter © 2012 Elsevier B.V. All rights reserved.
doi:10.1016/j.jpowsour.2012.01.149

Nomenclature

List of symbols

I	current, A
F	Faraday constant, 96,485 C equivalent^{-1}
H/M	atomic ratio of hydrogen to metal
n	number of moles
Δn	change in number of moles
N	number of moles
p	pressure, psi
R	Gas constant, J (mol K)$^{-1}$
t	time, s
T	temperature, K
V	volume, cm^3
Z	number of electrons transferred in a faradic reaction, equivalent mole^{-1}

Subscripts

discharge	discharge phase
H	hydrogen atom
H_2	hydrogen molecule
0	initial
MH	metal hydride

electrochemically active area for hydrogen oxidation/evolution reaction as a result of increased particle to particle contact resistance. Therefore it is necessary to formulate electrodes with a low molar volume of hydrogen or with a narrow plateau region in the pressure–composition isotherm.

In comparison, pulverization of the metal hydride particles in our low pressure Ni–H_2 cell does not affect the capacity or cycle life of the metal hydride. The smaller particles produced by pulverization are still active for the hydrogen absorption/desorption reaction which occurs through the interaction of hydrogen gas with the hydrogen storage material. Researchers have also shown that the addition of palladium enhances the kinetics of the hydrogen absorption/desorption reactions due to the electrocatalytic effect of palladium [20,21,25–27].

The pressure variations of the nickel hydrogen cell using the metal hydride, $LaAl_{0.3}Ni_{4.7}$ surface modified by Pd, for hydrogen storage will be analyzed here and a methodology to predict the state of charge (SOC) of the cell from the pressure will be presented.

2. Experimental

A nickel–hydrogen cell with metal hydride for hydrogen storage was assembled as shown in Fig. 1 of Part 1 of this paper. Nickel foam pasted with the metal hydride, 10 wt% Pd treated $LaNi_{4.7}Al_{0.3}$ by grinding, was placed at the end of the cell and was physically separated from the negative electrode by a chlorinated polyvinyl chloride disc. This minimizes contact of the KOH solution with the metal hydride. The hydrogen absorption characteristics of the metal hydride were tested in a Sievert's Apparatus [21] before use in the cell. The positive and negative electrodes and the separator and electrolyte were the same as in Part 1. The behavior of a nickel–hydrogen cell with an experimental capacity of 13.24 mA h cm^{-2} (positive electrode) will be discussed in this article. The experimental capacity of the positive electrode was determined in a flooded half-cell. The absolute capacity of the positive electrode was 72 mA h. The total capacity of the negative electrode for hydrogen oxidation (including the gas volume and metal hydride capacity) is 327 mA h at 1 atm pressure of which the metal hydride capacity is 241 mA h and rest is gaseous hydrogen.

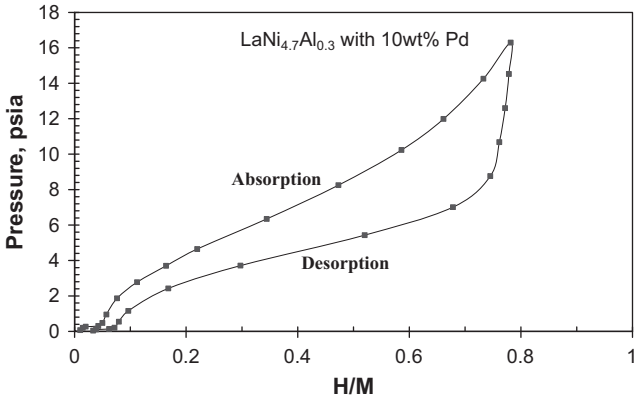

Fig. 1. Pressure–composition isotherm of the 10 wt% Pd modified $LaNi_{4.7}Al_{0.3}$ as measured with a Sievert's apparatus at 298 K [21].

Therefore the capacity of the positive nickel hydroxide electrode is limiting in comparison to that of the negative electrode.

After assembling the cell and placing it within the stainless steel pressure vessel, the pressure vessel was purged with N_2. This was followed by purging with hydrogen gas, and the metal hydride absorbed hydrogen according to the pressure composition isotherm. The final pressure of the cell at the end of this purge was about two atmospheres absolute pressure.

The cell was cycled at pressures above 1 atm to confirm the typical performance expected of the nickel hydroxide and platinum electrodes as discussed in Part 1 of this paper. Subsequently, after charging the nickel–hydrogen cell to 70% of full charge, the pressure was reduced by venting the cell into an evacuated chamber. This method was found to minimize the loss of electrolyte when lowering the cell pressure. The time constant for the hydrogen gas to equilibrate with the metal hydride in the Ni–H_2 cell after venting is about 0.1–0.2 h (Fig. 2A). This is similar to the time constant measured for equilibration of the metal hydride in our Sievert's apparatus, indicating that the cell configuration and assembly does not limit hydrogen access to the metal hydride.

3. Results and discussion

3.1. Pressure composition isotherm of the metal hydride

The pressure composition isotherm (PCI) of the metal hydride used in our Ni–H_2 cell, $LaAl_{0.3}Ni_{4.7}$ surface modified by Pd, is shown in Fig. 1. Test results showed that the metal hydride does not deactivate over 55 weeks in humid air [21] and the modified alloy is easily activated at sub-atmospheric pressures [20]. The hydrogen concentration in the alloy is expressed in terms of the atomic ratio of hydrogen to metal, H/M. As the hydrogen pressure is increased during absorption, the hydrogen concentration increases in the alloy. It can be seen in Fig. 1 that most of the absorption occurs below 1 atm absolute pressure. The pressure composition curve is higher during absorption indicating hysteresis under the test conditions used. The pressure composition curves for absorption and desorption were fitted using a polynomial to predict the hydrogen concentration in the alloy for a given pressure. For absorption, the polynomial fit is:

for $2.7 \le p \le 16.3$ psi,

$$\frac{\mathrm{H}}{\mathrm{M}} = 3.14 \times 10^{-5} p^4 - 1.33 \times 10^{-3} p^3 + 1.71 \times 10^{-2} p^2 - 1.85 \times 10^{-2} p + 5.77 \times 10^{-2} \quad (1)$$

For desorption, the polynomial fits over two ranges are:

for $8.75 \le p \le 16.3$ psi

$$\frac{H}{M} = -5.81 \times 10^{-4}p^2 + 1.93 \times 10^{-2}p + 6.21 \times 10^{-1} \quad (2)$$

for $2.4 \le p < 8.75$ psi

$$\frac{H}{M} = 3.17 \times 10^{-4}p^4 - 9.86 \times 10^{-3}p^3 + 9.44 \times 10^{-2}p^2 - 2.34 \times 10^{-1}p + 3.11 \times 10^{-1} \quad (3)$$

3.2. Theoretical pressure calculations based on the pressure–composition isotherm

The contribution of the hydrogen atoms from the gas phase is calculated based on the ideal gas law:

$$\Delta n_{H_2}(p) = \frac{2 \times (p_0 - p)V}{RT} \quad (4)$$

where p_0 is the initial pressure at the beginning of discharge, p is the pressure at any point during the discharge, V is the volume of gas in the cell (42 cm^3), R is the gas constant and T is the absolute temperature (25 °C). The effect of temperature variation inside the battery on changes in pressure is considered negligible in comparison to the pressure changes due to the hydrogen evolution. A factor of 2 is used to convert the number of moles of hydrogen molecules to the number of moles of hydrogen atoms, since the PCI behavior is expressed in terms of hydrogen atoms.

The contribution of the hydrogen from the metal hydride phase is obtained from either the desorption or absorption curves of the pressure composition isotherm. The number of hydrogen atoms consumed from the metal hydride is given as:

$$\Delta n_{MH}(p) = \left(\frac{H}{M_0} - \frac{H}{M}\right) \times N_{MH} \times 6 \quad (5)$$

where H/M_0 is the number of hydrogen atoms per metal atom corresponding to the initial pressure, P_0, at the beginning of discharge, H/M is the number of hydrogen atoms per metal atom corresponding to pressure, P, at any given time, N_{MH} is the number of moles of the metal hydride available measured using the Sieverts apparatus, 9.64×10^{-4} moles, and the factor, 6, corresponds to the six metal atoms per mole of metal hydride. The number of hydrogen atoms per metal atom is calculated from Eqs. (2) and (3) corresponding to the desorption part of the pressure composition isotherm, or from Eq. (1) for the absorption part of the PCI.

During discharge, the number of moles of hydrogen atom required for oxidation, $n_{H,discharge}(t)$ is given by Faraday's Law:

$$n_{H,discharge}(t) = \frac{It}{ZF} \quad (6)$$

where I is the discharge current of the battery, t is the time of discharge, Z is the number of electrons per equivalent, 1 (for the oxidation of hydrogen atom) and F is the Faradaic constant, 96,485 C equivalent^{-1}.

The total number of hydrogen atoms oxidized is the sum of hydrogen utilized from the gas phase and the metal hydride phase is expressed below:

$$n_{H,discharge}(t) = \Delta n_{H_2}(p) + \Delta n_{MH}(p) \quad (7)$$

Solving Eq. (7) with Eqs. (2)–(6) for a given discharge time, the theoretical pressure during charge or discharge can be calculated.

3.3. Pressure variation analysis in the range: 8–13 psia

After the initial assembly and check-out at pressures above 1 atm, the cell was vented as described above. The cell was then discharged completely to a cut-off voltage of 1.15 V at a C/5 rate. The pressure measured during the subsequent rest period after discharge at the sub-atmospheric pressure is shown in Fig. 2B. The pressure decreases during discharge as expected because of hydrogen oxidation at the platinum electrode. Fig. 2B shows that the pressure increases during the rest period after discharge. This indicates that the hydrogen in the gas phase is not in equilibrium with hydrogen in the metal hydride at the end of discharge. The time for equilibration is 1–2 h. Comparing Fig. 2A and B, it is clear that the hydrogen equilibration time for this Ni–H_2 cell construction is a function of the pressure inside the cell. The equilibration time is shorter when the pressure is higher. This is because the change in the amount of hydrogen sorbed into the metal hydride in the pressure range, 8–17 psia, is small whereas the change in amount of hydrogen desorption in the pressure range, 1–8 psia, is significant (see Fig. 1).

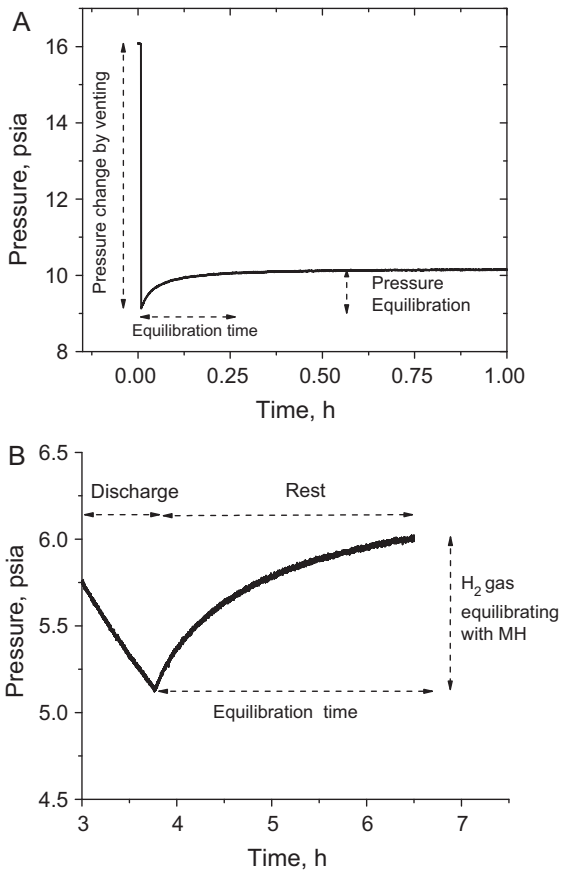

Fig. 2. Hydrogen gas equilibration with metal hydride at different pressures. (A) Pressure variation during and after venting following assembly and testing at about 1 atm. (B) Pressure variation during rest period at lower pressure following discharge.

The coulometric efficiency of the cell containing the metal hydride was investigated at different depths of charge and different rest periods to evaluate oxygen evolution during charge and the self-discharge mechanism during the rest period after charging. The cell was cycled at a C/5 rate to different states of charge, 50, 70 and 90%, from a fully discharged state with different rest periods (5 min, 1 h and 6 h) and the efficiencies are shown in Table 1. The discharge cut-off voltage is 1.15 V. The voltage profile during the charge is similar to the Ni–H_2 cell without metal hydride as discussed in Part 1 of this paper. The coulometric efficiency of the cell with metal hydride was calculated as the ratio of the charge delivered during discharge divided by the charge injected during charging. The coulometric efficiency was found to agree closely with that of

Table 1
Coulometric efficiency of the Ni–H_2 cell as a function of SOC cycled at C/5 rate.

SOC, %	Efficiency for different rest periods (%)		
	5 min	1 h	6 h
50	95.0	93.5	87.3
70	93.1	92.1	86.4
90	90.7	89.7	85.4

Ni–H_2 cell without the metal hydride. The coulometric efficiency decreases with increasing SOC for all rest periods indicating that oxygen evolution increases with SOC, similar to the results obtained for the nickel–hydrogen cell without metal hydride. The coulometric efficiency also decreases with increases in the rest period for different states of charge indicating that self discharge is occurring in the nickel–hydrogen cell. Self-discharge in the Ni–H_2 cell with metal hydride will be compared to the cell without metal hydride below.

The pressure variation during charge–discharge of the nickel–hydrogen cell with metal hydride cycled at a C/5 rate to a 50% SOC is shown in Fig. 3 for pressures between 8 and 13 psia. The rest period after charge and after discharge was 1 h. The pressure variation during charge and discharge is similar to that observed for the nickel–hydrogen cell without the metal hydride. No increase in pressure is observed during the rest period following the discharge as show in Fig. 3 confirming that the time for hydrogen equilibration with metal hydride is small for higher pressures as noted in Fig. 2A.

For a C/5 charge rate, the rate of pressure rise corresponding to the hydrogen formation at the platinum electrode calculated based on Faraday's law and the ideal gas law is 2.30 psi h^{-1} (when there is no MH). However, part of the hydrogen formed is absorbed into the metal hydride and therefore the rate of pressure change should be lower than 2.30 psi h^{-1}. The pressure variations during charge and discharge were fitted linearly as shown in Fig. 3. The pressure rate during charge and discharge is 1.84 psi h^{-1} and 1.94 psi h^{-1}, respectively. During discharge, the decrease in the pressure rate is due to the utilization of hydrogen from the metal hydride phase in addition to that from the gas phase. However the non-linear pressure–time behavior observed during the end of charge for the Ni–H_2 cell without the metal hydride (as discussed in Part 1 of this paper) is not evident in Fig. 3. This does not mean that there is not oxygen evolution and recombination occurring at the end of charging phase. The coulometric efficiency of the cell under these conditions was 92.2%, which indicates an efficiency loss due to oxygen evolution. However, the combination of hydrogen absorption into the metal hydride with oxygen evolution during charging makes it difficult to calculate isolate pressure changes due to oxygen evolution and recombination during and after charging.

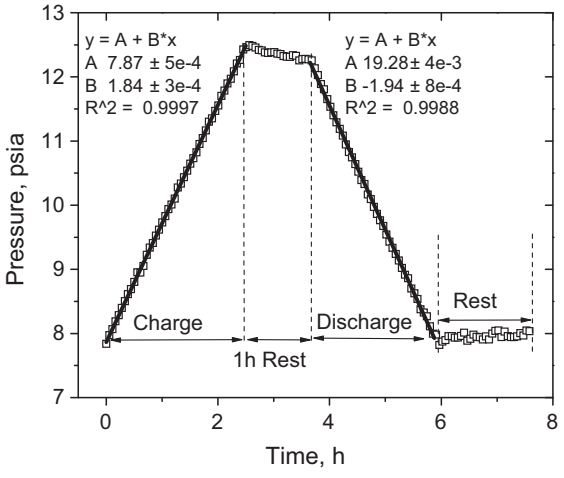

Fig. 3. Changes in pressure during the charge, the rest and the discharge periods of a cycle. The cell was cycled at C/5 rate from 0 to 50% SOC. The rest period for the cycle is 1 h. Linear fits of the pressure variations during charge and discharge are shown.

3.3.1. Correlation of pressure variations during charge and discharge to pressure composition isotherm – fuel gauging for pressures between 8 and 13 psia

The coulometric efficiency for the cycle to 50% SOC with a 1 h rest period as shown in Fig. 3 is 92.2%. Based on this efficiency, the SOC of the cell at the beginning of discharge is estimated as 46.1% instead of the intended 50% because of oxygen evolution during charge and self discharge during the 1 h rest period following charge. The pressure variation and amounts of hydrogen utilized from the gas phase and MH sources as a function of the discharge time were calculated utilizing the pressure composition isotherm and Eqs. (4)–(7) given above. The predicted pressure and the actual pressure measured during discharge are compared in Table 2. The calculated theoretical pressure agrees well with the measured pressure at different discharge times when the theoretical pressure is based on the desorption part of the PCI curve. This clearly indicates that the pressure inside the Ni–H_2 cell during a C/5 discharge follows the desorption curve of the pressure composition isotherm and can be used to gauge the hydrogen available in the metal hydride. Based on this analysis, the SOC of the battery can be calculated from the measured pressure and vice versa. Table 2 also shows the percentage amount of hydrogen utilized from the gaseous phase and from the metal hydride phase at different states of charge. The contribution of hydrogen from the metal hydride phase is about four times less than that of the hydrogen from the gas phase. This is because the change in number of hydrogen atoms per metal atom concentration in this pressure range (8–13 psia) is small as seen in Fig. 1.

A similar analysis was performed for charging the battery from a completely discharged state to 50% SOC. In this case, the theoretical pressure was calculated based on both the absorption and desorption portions of the PCI shown in Fig. 1 and the results were compared to the experimentally measured pressure as listed in Tables 3 and 4. From the comparisons shown in Tables 3 and 4, it is clear that during charge the pressure follows the desorption part of the PCI curve. This suggests that the desorption part of the curve shown in Fig. 1 follows the true equilibrium behavior, and that the hysteresis seen between absorption and desorption due to non-equilibrium behavior is reflected in the absorption data alone.

3.4. Pressure variations analysis in the pressure range: 6–12 psia

The pressure variation during two successive cycles of the nickel–hydrogen cell in the pressure range, 6–12 psia is shown in Fig. 4. The cell was cycled at a C/5 rate from a fully discharged state to 70% SOC and back. The rest period after charge and after discharge for the first cycle was 5 min. During the second cycle the rest periods were 6 h. The cell pressure behavior during charge and discharge was generally similar to that observed for the nickel–hydrogen cell in the operational pressure range 8–13 psia. However, there are differences between the two cycles shown in Fig. 4 in comparison to the cycle operated in the pressure range from 8 to 13 psia (Fig. 3). These differences are primarily seen in the pressure variations seen during the rest periods, and are a consequence of the slower hydrogen equilibration with the metal hydride at lower hydrogen pressures.

3.4.1. Pressure variations during rest after discharge

The pressure during the 6 h rest period at the end of the 2nd discharge rises to a higher value as shown in Fig. 4 and in more

Table 2
Change in various parameters following the desorption curve of the pressure composition isotherm for discharge in the pressure range 8–13 psia.

Discharge time (h)	SOC (%)	Theoretical pressure (psia)	Hydrogen from MH (%)	Hydrogen, from gas (%)	Total hydrogen utilized (mmoles)	Measured pressure (psia)
0	46.1	12.28	0.0	0.0	0.00	12.28
0.5	36.1	11.23	12.9	87.1	0.27	11.20
1	26.1	10.21	14.0	86.0	0.54	10.23
1.5	16.1	9.20	15.1	84.9	0.81	9.26
2	6.1	8.27	17.0	83.0	1.07	8.36
2.3	0.0	7.86	20.6	79.4	1.24	7.86

Table 3
Change in various parameters following the absorption curve of the pressure composition isotherm for charge in the pressure range 8–13 psia.

Charge time (h)	SOC (%)	Theoretical pressure (psia)	Hydrogen into MH (%)	Hydrogen as gas (%)	Total hydrogen evolved (mmoles)	Measured pressure (psia)
0	0.0	7.83	0.0	0.0	0.00	7.84
0.5	10.0	8.27	62.9	37.1	0.27	8.81
1	20.0	8.73	62.4	37.6	0.54	9.72
1.5	30.0	9.21	61.8	38.2	0.81	10.63
2	40.0	9.70	61.2	38.8	1.07	11.56
2.44	48.7	10.14	60.3	39.7	1.31	12.49

Table 4
Change in various parameters following the desorption curve of the pressure composition isotherm for charge in the pressure range 8–13 psia.

Charge time (h)	SOC (%)	Theoretical pressure (psia)	Hydrogen from MH (%)	Hydrogen, from gas (%)	Total hydrogen evolved (mmoles)	Measured pressure (psia)
0	0.0	7.83	0.0	0.0	0.00	7.84
0.5	10.0	8.55	40.2	59.8	0.27	8.81
1	20.0	9.53	29.3	70.7	0.54	9.72
1.5	30.0	10.54	25.1	74.9	0.81	10.63
2	40.0	11.57	22.4	77.6	1.07	11.56
2.44	48.7	12.49	20.6	79.4	1.31	12.49

detail in Fig. 5. It is noted that there is no oxygen evolution during discharge and therefore no recombination occurring at the end of discharge to cause a change in pressure. As discussed earlier and shown in Fig. 2B, it is evident that the hydrogen equilibration with metal hydride is slower at pressures on the order of 6 psia because of the significant amount of hydrogen absorption into the metal hydride that has to occur, following the pressure composition isotherm (Fig. 1). Therefore it is likely that this pressure rise during the rest period is related to slow hydrogen equilibration (slow hydrogen desorption/absorption) with the metal hydride. This is also supported by the fact that the pressure measured at the end of the rest period, after the pressure rise, is equal to the pressure measured at the beginning of the 1st charge (Fig. 4), indicating that eventually equilibrium is obtained and the same pressure is found for the same SOC.

The time constant for the hydrogen to equilibrate with the metal hydride was estimated using an exponential fit as shown in Fig. 5. Oh et al. [28] have developed a model for the hydrogen absorption based on different rate controlling steps: (a) dissociative chemisorption of the hydrogen molecule; (b) diffusion of the hydrogen atoms through the metal hydride and (c) chemical reaction of the hydrogen atom with the hydride. Here we do not analyze which of these is a rate determining step and instead focus our attention

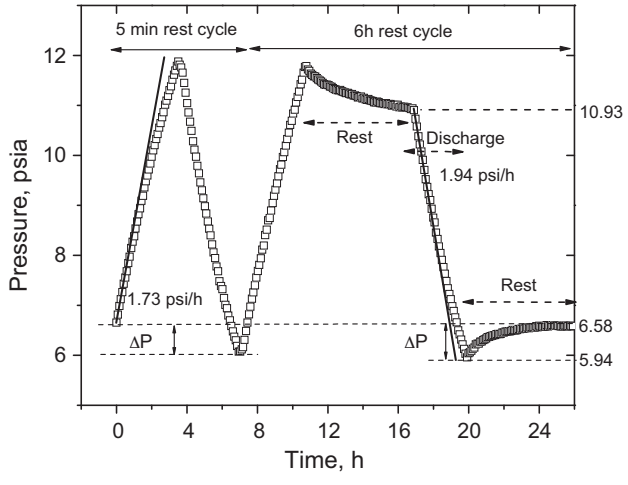

Fig. 4. Changes in pressure during the charge, the rest and the discharge periods of two successive cycles. The cell was cycled at C/5 rate to between 0 and 70% SOC. The rest periods for the 1st cycle and the 2nd cycle are 5 min and 6 h, respectively.

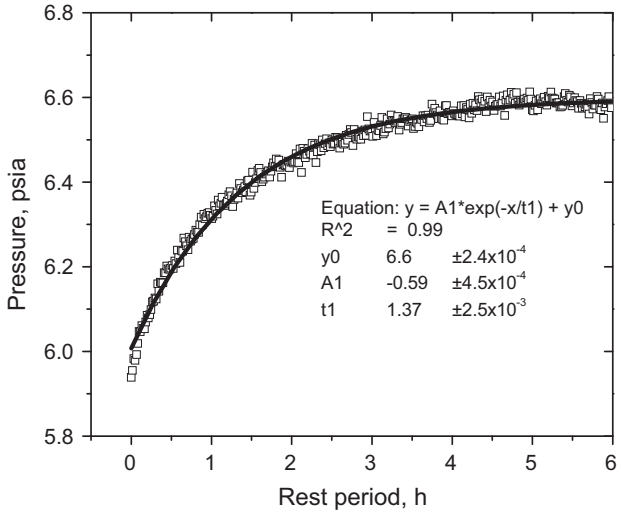

Fig. 5. Changes in pressure during the rest period at the end of the 2nd cycle shown in Fig. 4. The cell was cycled at C/5 rate from 0% to 70% and back to 0% SOC.

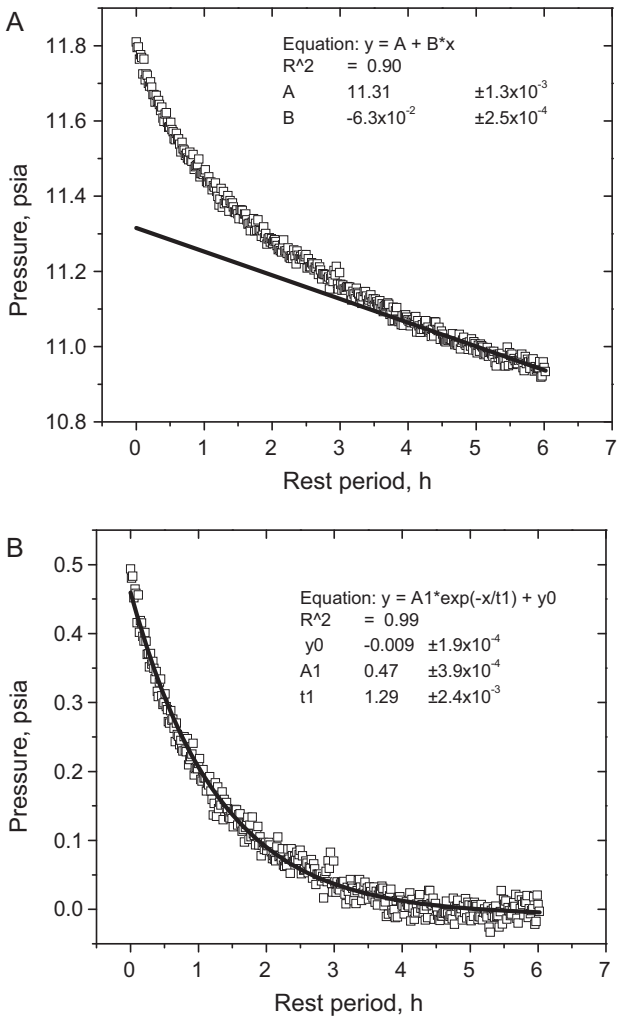

Fig. 6. Pressure changes during the 6 h rest period after the 2nd charge in Fig. 4. (A) A straight line is fit to the pressure data in the 4 to 6 h rest period and extrapolated back to time 0 h. (B) Estimated pressure changes due to recombination reaction and hydrogen equilibration with the metal hydride during the rest period after the 2nd charge. An exponential decay line is fit to the pressure data.

on estimating the overall time constant for hydrogen absorption. Shan et al. [21] have briefly reviewed the literature on the kinetics of hydrogen absorption in metal hydride. The exponential fit to the pressure–time data is reasonable and predicts the time constant for hydrogen absorption as 1.37 h at a pressure of 6 psia. In comparison, it is noted that the time constant of the metal hydride to equilibrate with hydrogen gas at the higher pressure range, 8–13 psia, is 0.1–0.2 h.

3.4.2. Pressure variations during rest after charge

The change in pressure during the rest period after the 2nd charge is shown in Fig. 6A. As discussed in Part 1 of this article, the pressure decrease during the rest period after charge is due to the recombination of oxygen with hydrogen and self discharge of the nickel hydroxide electrode consuming hydrogen gas. The self discharge occurs throughout the rest period, however, it was shown that the recombination reaction is complete within the first 1 h of the rest period. With metal hydride present, in addition to the self discharge and the recombination reaction during the rest period, there is also the hydrogen equilibration with the metal hydride to consider. Based on the analysis of the discharge data above, the time constant for the hydrogen equilibration with the hydride is 1.4 h or less. Therefore any changes in pressure observed for rest periods longer than about 1.5 h can be safely assumed to correspond to the self-discharge of the cell.

To estimate the self-discharge behavior, a straight line was fit to the pressure data in the time period of 4–6 h as shown in Fig. 6A. The rate of pressure change due to self-discharge is given by the slope of line (the parameter 'B') and is found to be 0.063 psi h^{-1}. This rate is about 37 times slower than the rate of pressure rise due to a C/5 charging rate (2.33 psi h^{-1}). That is, if the self-discharge rate were to remain constant, the battery would discharge completely in about 185 h, i.e., the self-discharge rate can be expressed as C/185. However, the self-discharge rate is a function of SOC as discussed below and in practice a much longer time would be required for the battery to completely self-discharge.

In order to estimate the contributions to the pressure change after charge due to the recombination reaction and the hydrogen equilibration with the metal hydride, the pressure drop due to the self-discharge mechanism was subtracted out of the pressure vs time data based on the linear fit parameters. The remaining pressure variation is plotted in Fig. 6B. An exponential decay equation was fit to this data as shown in the figure. The estimated time constant is about 1.29 h. It is noted that the time constant for the recombination reaction as found in Part 1 of this paper and that of the hydrogen equilibration with the metal hydride are both on this time scale and therefore it is not possible to separate the pressure contributions due to these two mechanisms.

3.4.3. Correlation of pressure variations during charge and discharge to the pressure composition isotherm – fuel gauging

The pressure and other parameters as a function of the SOC of the cell were calculated as discussed in previous section using Eqs. (2)–(7) for the charge during the 1st cycle and discharge during the 2nd cycle shown in Fig. 4. These results are shown in Tables 5 and 6.

Since there is some oxygen evolution during charge, the coulometric efficiency is always less than 100%. With a 5 min rest after charging, the coulometric efficiency for a battery charged to 70% SOC is 92.9%. Based on this, the SOC of the cell at the end of charge is estimated at 65.1% instead of the intended 70%. The pressure variation for different states of charge during charging was estimated based on the desorption curve of the pressure composition isotherm is listed in Table 5. The calculated theoretical pressure is lower than the measured pressure during charge for all states of charge indicating that the hydrogen gas in the gas phase is not in equilibrium with the metal hydride. It is evident that the difference between the measured pressure and calculated theoretical pressure increases with SOC up to 30% SOC (theoretical pressure 8.08 psi) and then decreases with increasing SOC from 30 up to 65.1% SOC (theoretical pressure 11.48 psi). The increase in the pressure difference is associated with the significant changes in the H/M ratio in the pressure range from 6 to 8 psia and the subsequent narrowing of the pressure difference is associated with the relatively smaller changes in the H/M ratio in the pressure range (9–12 psia). The theoretical pressure calculated at 65.1% SOC (end of charge) is 11.48 psi and is lower than the pressure measured at the end of charge, 11.81 psi, and is above the pressure measured at the end of the rest period, 10.93 psi, due to the offsetting effects of oxygen evolution (increases pressure), hydrogen–oxygen recombination (lowers pressure) and slow hydrogen equilibration with the metal hydride (lowers pressure as equilibration is reached).

Because of the significant self-discharge during the 6 h rest period following charge the coulometric efficiency for the 2nd cycle was 86.4%. Thus, the SOC of the cell at the beginning of discharge was estimated at 60.5%.

For the first 1.5 h of the discharge the measured pressure change was 10.93–8.09 psia (Table 6). In this pressure range, there is no significant change in the H/M ratio in the metal hydride, and as listed in Table 6, the theoretical pressure calculated agrees well with the

Table 5
Change in various parameters following the desorption curve of the pressure composition isotherm for charge in the pressure range 6–12 psia.

Charge time (h)	SOC (%)	Theoretical pressure (psia)	Hydrogen from MH (%)	Hydrogen, from gas (%)	Total hydrogen evolved (mmoles)	Measured pressure (psia)
0.0	0.0	6.65	0.0	0.0	0.00	6.65
0.5	10.0	7.04	67.4	32.6	0.27	7.55
1.0	20.0	7.50	64.7	35.3	0.54	8.41
1.5	30.0	8.08	60.5	39.5	0.81	9.21
2.0	40.0	8.94	52.5	47.5	1.07	9.95
2.5	50.0	9.93	45.6	54.4	1.34	10.66
3.0	60.0	10.95	40.6	59.4	1.61	11.30
3.3	65.1	11.48	38.5	61.5	1.75	11.87

Table 6
Change in various parameters following the desorption curve of the pressure composition isotherm for discharge in the pressure range, 6–12 psia.

Discharge time (h)	SOC (%)	Theoretical pressure (psia)	Hydrogen from MH (%)	Hydrogen, from gas (%)	Total hydrogen utilized (mmoles)	Measured pressure (psia)
0.0	60.5	10.93	0.0	0.0	0.00	10.93
0.5	50.5	9.91	15.8	84.2	0.27	9.94
1.0	40.5	8.92	16.9	83.1	0.54	8.99
1.5	30.5	8.07	20.9	79.1	0.81	8.09
2.0	20.5	7.49	28.8	71.2	1.08	7.28
2.5	10.5	7.04	35.4	64.6	1.34	6.56
3.0	0.0	6.62	41.0	59.0	1.63	5.95

Table 7
Self discharge rate for different states of charge for Ni–H_2 cell with metal hydride.

% SOC	Self-discharge rate, psi h^{-1}
50	0.048
70	0.063
90	0.063

measured pressure inside the cell. Most of the hydrogen consumed up to this point was originally stored in the gas phase. This is why the actual rate of pressure drop measured, 1.94 psi h^{-1}, is close to that of 2.33 psi h^{-1}; the rate for the Ni–H_2 cell without metal hydride. However, it is evident from Fig. 4 that the rate of pressure change is non-linear toward the end of discharge (8–6 psia) in agreement with the fact that a significant amount of hydrogen is being released by the metal hydride phase at these pressures. At the end of discharge, about 41% of the total hydrogen oxidized at the platinum electrode was released from the metal hydride and the rest, 59%, was hydrogen initially stored in the gas phase. This significant change in the amount of hydrogen in the metal hydride phase increases the hydrogen equilibration time with the metal hydride, resulting in a lower measured pressure than that calculated for 20.5, 10.5 and 0% SOC. Given sufficient time for hydrogen equilibrate with the metal hydride, the pressure measured at the end of the rest period after discharge, 6.58 psi, agrees with the calculated theoretical pressure at 0% SOC, 6.62 psi (Table 6). Again, the pressure inside the Ni–H_2 cell during discharge follows the desorption curve of the pressure composition isotherm.

3.5. Self-discharge at different states of charge

The self-discharge rate was estimated based on the linear fit on the pressure data in the 4–6 h rest period after charge as discussed previously for several states of charge and is listed in Table 7. It is evident that the self-discharge rates at 70 and 90% SOC are the same and are greater than that at the 50% SOC. The self-discharge rate of the cell with metal hydride is C/185 at 90% SOC. In comparison, the self discharge rate of the Ni–H_2 cell without metal hydride is C/90. The difference is due to the different pressures used. The cell with metal hydride is operated at lower pressures and as a result the self-discharge rate is lower.

4. Conclusions

A nickel–hydrogen cell with metal hydride for hydrogen storage was assembled and tested successfully. The coulometric efficiency of the cell was studied for different states of charge and different rest periods. The coulometric efficiency decreases with increasing SOC due to oxygen evolution as a side reaction. The coulometric efficiency also decreases with increasing rest period following charge because of self-discharge of the cell. These results are the same as those observed in the cell without the metal hydride.

Pressure vs time data measured during cycling was analyzed. In addition to the variables: oxygen evolution, recombination reaction and self discharge for the cell, the use of metal hydride for hydrogen storage introduces another variable, the equilibration of hydrogen with the metal hydride. It was shown that equilibration with the metal hydride is faster when cell is operated in the pressure range 8–13 psia and is slower when operated in the pressure range 6–12 psia because of significant hydrogen absorption/desorption below 8 psi pressure. The time constant in the case of slow hydrogen equilibration with the metal hydride is about 1.37 h, similar to the time constant for the recombination reaction, making it difficult to separate the pressure contributions due to these mechanisms. The self discharge rate, however, was obtained using a linear fit at longer rest times after charge.

The pressure–time behavior during charge and discharge of the battery were found to follow the desorption part of the pressure composition isotherm very well. Based on the measured pressure and the pressure composition isotherm, the hydrogen available in the cell can be easily gauged and the SOC of the cell can be predicted for cells. For cells with slow hydrogen equilibration, a sufficient rest period needs to be used to accurately predict the SOC. This indicates that the hydrogen equilibration kinetics with the metal hydride needs to be significantly improved to monitor the performance of the low pressure Ni–H_2 cells in real time.

Acknowledgment

This research was supported by NIH grant, NINDS R02-NS41809.

References

[1] P. Dantzer, Top. Appl. Phys. 73 (1997) 279–340.

[2] S.K. Dhar, S.R. Ovshinsky, P.R. Gifford, D.A. Corrigan, M.A. Fetcenko, S. Venkatesan, J. Power Sources 65 (1997) 1–7.
[3] O.A. Petrii, S.Y. Vasina, I.I. Korobov, Usp. Khim. 65 (1996) 195–210.
[4] G. Wojcik, M. Kopczyk, Wiadomosci Chemiczne 49 (1995) 285–299.
[5] A. Anani, A. Visintin, K. Petrov, S. Srinivasan, J.J. Reilly, J.R. Johnson, R.B. Schwarz, P.B. Desch, J. Power Sources 47 (1994) 261–275.
[6] M.A. Fetcenko, S. Venkatesan, S.R. Ovshinsky, Proc. – Electrochem. Soc. 92–5 (1992) 141–167.
[7] T. Sakai, K. Muta, H. Miyamura, N. Kuriyama, H. Ishikawa, Proc. – Electrochem. Soc. 92–5 (1992) 59–91.
[8] C. Iwakura, M. Matsuoka, Prog. Batteries Solar Cells 10 (1991) 81–114.
[9] H.F. Bittner, C.C. Badcock, J. Electrochem. Soc. 130 (1983) 193C–198C.
[10] K. Hong, J. Power Sources 96 (2001) 85–89.
[11] S.R. Ovshinsky, M.A. Fetcenko, J. Ross, Science 260 (1993) 176–181.
[12] J. Kleperis, G. Wojcik, A. Czerwinski, J. Skowronski, M. Kopczyk, M. Beltowska-Brzezinska, J. Solid State Electrochem. 5 (2001) 229–249.
[13] F. Feng, M. Geng, D.O. Northwood, Int. J. Hydrogen Energy 26 (2001) 725–734.
[14] Z. Zhou, J. Yan, Y. Li, D. Song, Y. Zhang, J. Power Sources 72 (1998) 236–238.
[15] P. Ruetschi, F. Meli, J. Desilvestro, J. Power Sources 57 (1995) 85–91.
[16] J.J.G. Willems, K.H.J. Buschow, J. Less-Common Metals 129 (1987) 13–30.
[17] H.J. Park, N.H. Goo, K.S. Lee, J. Electrochem. Soc. 150 (2003) A1328–A1332.
[18] T. Ma, Y. Hatano, T. Abe, K. Watanabe, J. Alloys Compd. 391 (2005) 313–317.
[19] P. Leblanc, C. Jordy, B. Knosp, P. Blanchard, J. Electrochem. Soc. 145 (1998) 860–863.
[20] X. Shan, D.L.J.S. Wainright, J.H. Payer, J. Power Sources 196 (2011) 827–834.
[21] X. Shan, J.S. Wainright, J.H. Payer, J. Alloys Compd. 430 (2007) 262–268.
[22] J.S. Wainright, J. Payer, C.C. Liu, L., Dudik, X., Shan, S. Levine, U.S. Patent #7,404,842 (July) (2008).
[23] Y. Nakamura, K. Sato, S. Fujitani, K. Nishio, K. Oguro, I. Uehara, J. Alloys Compd. 267 (1998) 205–210.
[24] G. Zheng, B.N. Popov, R.E. White, J. Appl. Electrochem. 28 (1998) 381–385.
[25] A. Visintin, C.A. Tori, G. Garaventta, W.E. Triaca, J. Electrochem. Soc. 145 (1998) 4169–4172.
[26] R.C. Ambrosio, E.A. Ticianelli, Surf. Coat. Technol. 197 (2005) 215–222.
[27] D. Barsellini, A. Visintin, W.E. Triaca, M.P. Soriaga, J. Power Sources 124 (2003) 309–313.
[28] J.W. Oh, C.Y. Kim, K.S. Nahm, K.S. Sim, J. Alloys Compd. 278 (1998) 270–276.